

Geophysical Research Letters

RESEARCH LETTER

10.1029/2020GL090542

Special Section:

The COVID-19 pandemic: linking health, society and environment

Key Points:

- Heavy haze still engulfed northern China despite great emission reductions during COVID-19 lockdown
- Enhanced secondary aerosols and decreased black carbon (BC) led to a more scattering atmosphere and weakened aerosol-planetary boundary layer interaction
- Observational evidences and quantitative modeling confirmed the importance of BC during the unique natural experiment

Supporting Information:

- Supporting Information S1

Correspondence to:

X. Huang,
xinhuang@nju.edu.cn



Citation:

Wang, Z., Huang, X., Ding, K., Ren, C., Cao, L., Zhou, D., et al. (2021). Weakened aerosol-PBL interaction during COVID-19 lockdown in northern China. *Geophysical Research Letters*, 48, e2020GL090542. <https://doi.org/10.1029/2020GL090542>

Received 31 AUG 2020

Accepted 21 DEC 2020

Weakened Aerosol-PBL Interaction During COVID-19 Lockdown in Northern China

Zilin Wang^{1,2}, Xin Huang^{1,2} , Ke Ding^{1,2}, Chuanhua Ren^{1,2}, Lu Cao³, Derong Zhou^{1,2}, Jian Gao⁴, and Aijun Ding^{1,2} 

¹School of Atmospheric Sciences, Nanjing University, Nanjing, China, ²Collaborative Innovation Center of Climate Change, Nanjing, Jiangsu Province, China, ³Meteorological Observatory of Jiangsu Province, Nanjing, China, ⁴Chinese Research Academy of Environmental Science, Beijing, China

Abstract Anthropogenic emissions were greatly constrained during COVID-19 lockdown in China. Nevertheless, observations still showed high loadings of fine particles (PM_{2.5}) over northern China with secondary aerosols increasing by 15 μg/m³ yet a ~10% drop in light-absorbing black carbon (BC). Such a chemical transition in aerosol composition tended to make the atmosphere more scattering, indicated by satellite-retrieved aerosol absorption optical depth falling by 60%. Comparison between weather forecast and radiosonde observations illustrated that, without upper-level heating induced by BC, the stabilized stratification diminished, which was conducive for planetary boundary layer (PBL) mixing and thus near-surface pollution dispersion. Furthermore, coupled dynamic-chemistry simulations estimated that emission reduction during the lockdown weakened aerosol-PBL interaction and thus a reduction of 25 μg/m³ (~50%) in PM_{2.5} enhancement. Based on the unique natural experiment, this work observationally confirmed and numerically quantified the importance of BC-induced meteorological feedback, further highlighting the priority of BC control in haze mitigation.

Plain Language Summary Atmospheric scattering and absorbing aerosols can both reduce sunlight reaching the earth surface, resulting in a surface cooling. Absorbing aerosols can also warm the upper air by trapping solar energy in the atmosphere. Such an opposite-changing temperature tendency in these two levels leads to a stable air mass, which is conducive for pollutant accumulation and air quality deterioration. Due to the emission reduction during COVID-19 lockdown, secondary scattering aerosols increased yet absorbing aerosols from primary emission decreased, accompanied with less stable air masses in the lower atmosphere. The reduced stability indicates that absorbing aerosols play a dominant role in suppressing boundary layer development and aggravating near-surface pollution accumulation. Thus, further efforts devoted to emission reduction of absorbing aerosols like black carbon may serve as an efficient approach for pollution mitigation.

1. Introduction

The outbreak of Coronavirus Disease 2019 (COVID-19) since the end of January 2020 has caused millions of affections and greatly influences social activities worldwide (Zhu et al., 2020). Strict restrictions on transportation and economic activities were implemented in many countries around the world, drastically changing anthropogenic emissions of primary pollutants. Recent studies have estimated that nitrogen oxides (NO_x) emission underwent a reduction of around 50% in eastern China and the column nitrogen dioxide (NO₂) dropped by over 20% and 30% in Western Europe and the United States, respectively (Bauwens et al., 2020; Zhang et al., 2020). At the same time, the concentration of carbon monoxide (CO) and organic aerosols from primary emissions also significantly declined associated with limited industrial activities (Chen et al., 2020; Filonchyk et al., 2020).

However, the air quality in northern China did not improve prominently due to reduced emissions as expected. Instead, extreme particulate matter levels and high concentrations of ozone (O₃) were recorded during the quarantine period in Beijing–Tianjin–Hebei area (BTH, Nichol et al., 2020; Sun et al., 2020). Several reasons have been considered to take responsibility for the unexpected pollution. Based on measurements and model simulations, the enhancement of secondary pollution under unbalanced emission cut-down was shown to cause the haze formation (Huang et al., 2020a; Pei et al., 2020). In particular, reduced

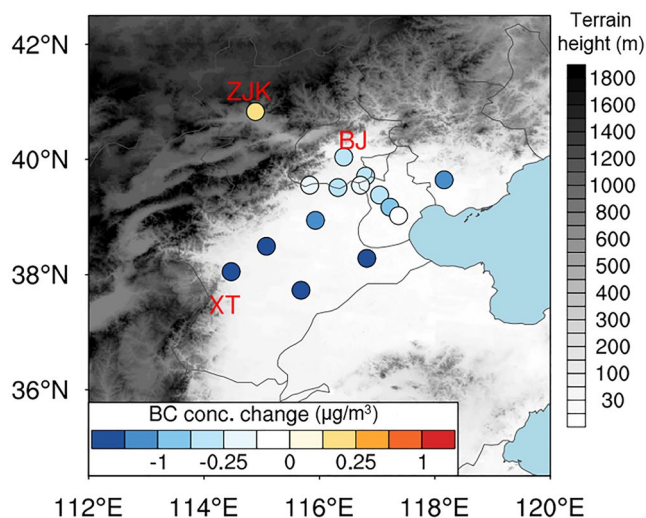


Figure 1. Topography of northern China and geographic location of stations measuring $PM_{2.5}$ chemical composition over BTH symbolized by dots. Colors of dots represent BC average concentration change between prelockdown and lockdown period. BJ (Beijing), XT (Xingtai), and ZJK (Zhangjiakou) with sounding observations are also marked in red on the map. BTH, Beijing–Tianjin–Hebei area; BC, black carbon.

NO_x emission weakened the titration effect, resulting in more O_3 near the ground surface (N. Wang et al., 2019). The elevated oxidizing capacity of atmosphere thus facilitated the formation of secondary aerosols. High humidity and stagnant meteorology also contributed to aerosol heterogeneous reactions and pollutants accumulation (P. Wang et al., 2020).

Contrary to increasing secondary pollutants, black carbon (BC), as a short-lived yet strong climate forcer, exhibited a remarkable decrease. The mass concentration of BC was reported to show a 22% decline in Beijing during the COVID-19 lockdown (Sun et al., 2020). Through absorption of solar radiation, BC could greatly perturb radiative transfer and energy budget of the earth system (Bond et al., 2013). The climate forcing of BC could reach as high as $+8.7 W/m^3$ in regions with huge fossil fuel combustion like China, significantly warming the atmosphere (Huang et al., 2015). With BC heating above as well as all aerosols reducing insolation at surface, the planetary boundary layer (PBL) is less energized in terms of buoyancy. In addition, upper-level warming and surface cooling by aerosols efficiently suppress turbulent motion and PBL evolution. Such poorly developed PBL trapping atmospheric pollutants within a shallower layer deteriorates air quality and triggers positive feedback between aerosol and boundary layer meteorology, namely aerosol-PBL interaction (A. J. Ding et al., 2016).

The aerosol-PBL interaction and its profound roles in haze formation and accumulation have been widely discussed and thoroughly explored (Huang et al., 2020b; Z. Li et al., 2017; Miao et al., 2017; Z. Wang

et al., 2018). Though some numerical studies indicate the vital role of BC in aerosol-PBL interaction (Z. Wang et al., 2018), the relative contribution from scattering and light-absorbing aerosols is still a question under debate. The sharply depressed human activities after COVID-19 outbreak pronouncedly changed the aerosol composition, which provided a special opportunity to investigate the contribution of aerosol-PBL interaction to haze pollution under different emission scenarios, and how anthropogenic emission reduction could impact this feedback. By integrating multi-based observations and numerical simulations, the effects of varying emission on aerosol-PBL interaction during COVID-19 lockdown are clearly demonstrated and quantified. Section 2 gives descriptions of applied data and numerical experiments. Section 3 presents the main results and conclusions are summarized in Section 4.

2. Observational Data and Numerical Experiments

2.1. Satellite and In Situ Observations

The MODIS Aerosol Products using Deep Blue algorithm from Terra (MOD04_L2) are adopted in this study. Daily level-2 aerosol optical depth (AOD) at 550 nm and single scattering albedo (SSA) at 470 nm with 10×10 km spatial resolution are collected to derive the optical properties of atmospheric column before and after the lockdown implemented.

Atmospheric sounding data are acquired from the radiosonde network of the L-band sounding system running by China Meteorological Administration. The network consists of 120 operational radiosonde stations in China with three of them locating at BTH including Beijing (BJ, 39.93°N, 116.28°E), Xingtai (XT, 37.18°N, 114.36°E), and Zhangjiakou (ZJK, 40.78°N, 114.88°E). Only data from BJ and XT were analyzed and ZJK is excluded due to its elevation (Figure 1). Fine-resolution profiles of temperature, relative humidity, pressure, and wind are detected and then interpolated to significant pressure levels (e.g., 1,000, 900, and 850 hPa) twice a day at 00 and 12 UTC.

Major atmospheric pollutants including particulate matter ($PM_{2.5}$ and PM_{10}), O_3 , CO, sulfur dioxide (SO_2), and NO_2 are recorded every hour at 80 air quality monitoring stations at BTH and released by Ministry of Ecology and Environment of People's Republic of China. Chemical compositions of fine particles recorded by Monitor for Aerosols and Gases in Ambient air at 15 sampling sites are utilized to investigate the difference in aerosol composition before and during the lockdown.

2.2. Weather Research and Forecast Model With Chemistry Configuration and Experimental Design

Weather Research and Forecast Model with Chemistry (WRF-Chem) version 4.0 is utilized to perform contrast experiments of emission cut-down (CUT) and fixed emission (noCUT) scenarios. As a fully coupled meteorology–aerosol–radiation–cloud model, WRF-Chem has been successfully applied in tremendous feedback studies (Chapman et al., 2009; Forkel et al., 2012; G. Grell et al., 2011). The major physical schemes used include Noah land surface scheme (Ek et al., 2003) and Grell cumulus parameterization (G. A. Grell & Dévényi, 2002) along with Lin microphysics (Lin et al., 1983). Rapid Radiative Transfer Model shortwave and longwave radiation scheme (RRTMG, Iacono et al., 2008) combined with Yonsei University PBL scheme (YSU, Hong et al., 2006) is applied to describe aerosol–radiation/PBL interaction. Photolytic reaction rates are derived using Fast-J photolysis scheme (Fast et al., 2006). Carbon Bond Mechanism version Z and Model for Simulating Aerosol Interactions and Chemistry including 11 aerosol species are used to represent gas phase and aerosol chemistry (Zaveri & Peters, 1999; Zaveri et al., 2008). Aerosols are separated into four bins (0.039–0.156, 0.156–0.625, 0.625–2.5, and 2.5–10 μm) according to their dry diameter. The assumptions of spherical particles and internally mixing are made in each bin to compute optical properties based on Mie theory.

The model domain covers eastern and northern China as well as its surrounding areas with a grid resolution of 20 km. Forty layers extend from the surface to model top are adopted following the optimized setting in Z. Wang et al. (2019). National Center for Environment Prediction global final analysis data (FNL) with a $1^\circ \times 1^\circ$ spatial resolution updated every 6 h provide initial and lateral boundary conditions for meteorological fields. The model simulation starts on December 25, 2019 while ends on February 10, 2020, leaving the first 5-day integration as spin-up. Each run covers 48 h and the last 24 h output were kept for further analysis. Two sets of parallel experiments with noCUT and CUT emission inventory are conducted under both feedback-included (FB) and feedback-excluded (noFB) scenarios. The difference between FB and noFB is attributed to aerosol radiative effects and the indirect effect of aerosol is not included in either experiment. The Multi-resolution Emission Inventory for China of anthropogenic emissions including SO_2 , NO_x , CO, $\text{PM}_{2.5}$, $\text{PM}_{\text{coarse}}$, BC, organic carbon, and nonmethane volatile organic compounds from five sectors is employed the entire modeling time in noCUT simulations (M. Li et al., 2014). The emission reduction due to lockdown control is estimated based on dynamic economic and industrial activity levels provided by National Bureau of Statistics (Huang et al., 2020a) and is incorporated in CUT simulations since January 23, 2020. The detailed method and emission reduction distribution is recorded in Supporting Information (Text S1, Figure S1). Further, another set of experiments with all emission cut-down except for BC (CUT_exBC) is performed to explore the relative contribution from absorbing aerosols and other aerosol components to the aerosol-PBL interaction. Table S1 summarized all the model experiments.

3. Results and Discussion

3.1. Changes in Aerosol Composition and Optical Properties

After the quarantine implemented in Wuhan on January 23, cities and provinces in China progressively issued movement restrictions since January 24, reflected by a 70% emission reduction from transport sector as well as a sudden decline in transportation index (Figures S1 and S2). The discharge of primary pollutants from industry such as cement production also decreased by about 30% due to the COVID-19 lockdown. Accordingly, average surface NO_2 over BTH decreased from 53 to 26 $\mu\text{g}/\text{m}^3$ as a result of strong constraints on traffic, which is the major contributor to atmospheric NO_x . SO_2 followed the decreasing trend of NO_2 but with a smaller magnitude since that the main source of SO_2 , namely coal consumption in power generation and heavy industries, did not show a decline as large as that in transportation (Zheng et al., 2020). Also, owing to the effectiveness of clean air actions in improving air quality executed from 2013 to 2017 (A. Ding et al., 2019), SO_2 has already dropped to a clean level with the average concentration lower than 20 $\mu\text{g}/\text{m}^3$. By contrast, O_3 and fine particles showed an opposite trend. The surface maximum daily 8-hour average O_3 was found to increase by 67% with the highest value of 62 and 83 $\mu\text{g}/\text{m}^3$ in two periods. Similarly, $\text{PM}_{2.5}$ rose to nearly the same level as that before the lockdown, as much as 160 $\mu\text{g}/\text{m}^3$. Both regional transport and enhanced chemical production contributed to the high levels of secondary pollutants (Chang et al., 2020; Huang et al., 2020a). An inverse relationship has been reported between $\text{PM}_{2.5}$ and O_3 in northern China

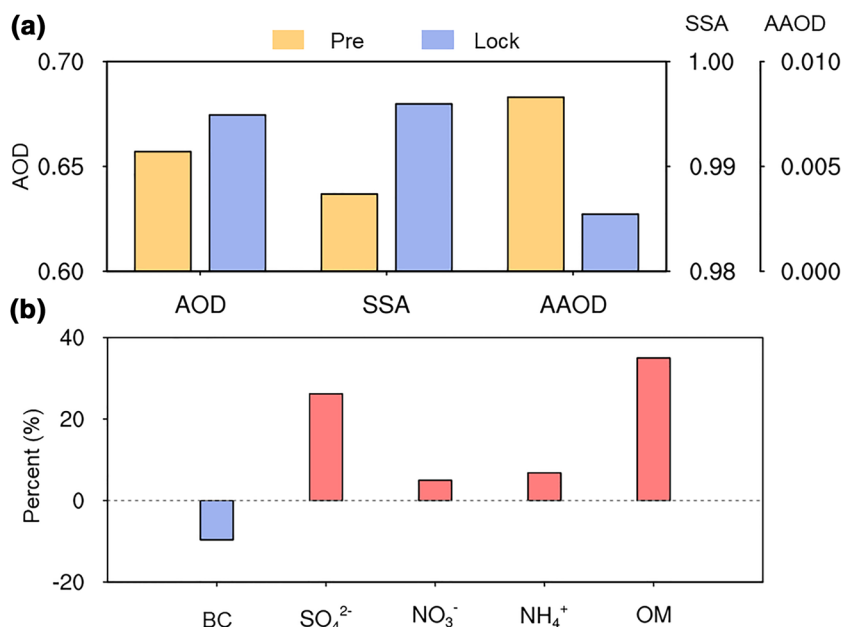


Figure 2. (a) MODIS observed average AOD, SSA, and AAOD over BTH average over prelockdown and lockdown period. (b) Relative change of various PM_{2.5} components over BTH between prelockdown and lockdown period according to in situ observations. SO₄²⁻, NO₃⁻, NH₄⁺, and OM represent sulfate, nitrate, ammonia, and organic matter/aerosols, respectively. AOD, aerosol optical depth; SSA, single scattering albedo; AAOD, aerosol absorption optical depth; and BTH, Beijing–Tianjin–Hebei area.

due to reduced photolysis by particle extinction or enhanced uptake of HO₂ radicals and O₃ precursors (Jia et al., 2017; K. Li et al., 2019). Such negative correlations hold true before the lockdown while work poorly in the pollution afterward.

Atmospheric aerosol components were monitored over BTH from the beginning of 2020 and all aerosol species exhibited great variations after the lockdown implemented (Figures 1 and 2b). For clarity, the prelockdown (Pre) hereafter is defined as the period between January 10 and 23 while lockdown (Lock) between January 24 and February 5. Notably, primary pollutants, like BC, decreased by approximately 10% average over BTH with a more pronounced drop in southern parts. Secondary aerosols including sulfate, nitrate, ammonia, and organic aerosols (SNAO), however, increased by 4, 2, 2, and 7 μg/m³, respectively, on average after the emission reduction caused by the lockdown. In particular, the increments in sulfate and organic aerosols exceeded 25%, contributing greatly to elevated PM_{2.5} concentrations. Comparatively, the increase of nitrate formation was less conspicuous due to dramatic fall of its gaseous precursor, NO_x (Fu et al., 2020). These changes are also confirmed by Huang et al. (2020a). As a result, the total secondary particulate matter, that is, SNAO versus BC showed an increasing trend from prelockdown to lockdown period (Figure S3), suggesting a rising portion of secondary species. Overall, secondary SNAO with scattering effect accounted for 80% and 93% of PM_{2.5} before and during the lockdown, while the fraction of primary absorbing BC decreased from 6% to 3%. Such a marked transformation in aerosol composition could greatly impact atmospheric optical properties.

Satellite-derived AOD and SSA can reflect important optical properties of atmospheric pollutants in the whole column (Figure S4). Compared with prelockdown period, the extinction of atmosphere weakened in southern and coastal areas of China, while intensified in central North China Plain (NCP), especially BTH, corresponding to more ambient scattering particles (Figure 2b). The average AOD over BTH increased from 0.657 to 0.674, accompanied with an enhancement of SSA, indicating a more scattering atmosphere. Such a transition in atmospheric optical properties was also confirmed by Diamond & Wood (2020) using linear regression model. The increment of SSA from 0.987 to 0.996 could be attributed to the drop of BC concentration as a strong light absorber (Ramanathan & Carmichael, 2008) as well as the increase in secondary aerosols as scattering species (Moise et al., 2015). Subsequently, the aerosol absorption optical depth (AAOD)

derived from $AAOD = AOD \times (1 - SSA)$ also experienced a tremendous falling from about 10×10^{-3} to 4×10^{-3} by over 60%. The significant alteration of aerosol optical properties could modify its interaction with radiation and thus boundary layer meteorology.

3.2. Disparities in Aerosol-PBL Interaction Due to Aerosol Composition Transition

Since aerosols' radiative effect is highly sensitive to optical properties depending on its chemical composition (Barnard et al., 2010; Z. Wang et al., 2018), such a transition in aerosol composition is expected to influence the intensity of its radiative forcing and subsequently aerosol-PBL interaction. To further investigate the aerosol-PBL interaction before and during quarantine, two heavily polluted episodes (EP1: January 17–18; EP2: January 26–27) were selected and compared. The meteorological conditions of both episodes were analogous with light wind (1–2 m/s) and moderate temperature around 0°C over BTH (Figure S5). BJ and XT were selected to conduct further analysis with basically the same $PM_{2.5}$ levels in two episodes. According to the temperature profiles from radiosonde and Global Forecast System (GFS) data set, real-time observations showed substantial atmospheric heating as well as surface cooling compared with weather forecast during prelockdown period (Figure 3). Since aerosols' feedback has not been included in GFS yet, the discrepancies between sounding and GFS data set could be attributed to aerosols partially (Huang et al., 2018). Under polluted conditions, atmospheric heating was mainly caused by absorbing aerosols and surface cooling resulted from reduced insolation by aerosol extinction of all chemical components (A. J. Ding et al., 2016). The upper-level heating reached over 2°C in XT and surface cooling could be as large as 5°C in BJ. Such an opposite change of temperature in these two levels led to a more stabilized and shallower boundary layer, indicating poorer ventilation and diffusion for near-surface pollutants. Through comparing FB and noFB WRF-Chem simulations, the stabilized stratification resulted from aerosol-PBL interaction is responsible for 80 $\mu\text{g}/\text{m}^3$ enhancement of surface $PM_{2.5}$ (~40% larger than noFB) during EP1 over BTH.

However, the impact of the feedback seems less significant in EP2. Although total $PM_{2.5}$ remained similar levels in EP1 and EP2, the upper-level heating in BJ and XT diminished, and the surface cooling was not so pronounced as well. The difference rooted in the changes of BC aerosols, which is the key factor of aerosol-PBL interaction (A. J. Ding et al., 2016; Z. Wang et al., 2018). First, the reduction of BC, both mass concentration and fraction (BC/ $PM_{2.5}$), resulted in less absorbing atmosphere, hence atmospheric heating is absent. Subsequently, without warming at higher altitudes, the temperature inversion greatly weakened, allowing more turbulent mixing and vertical transport. Therefore, near surface cooling was diffused and homogenized within the boundary layer, leading to scarce or slight cooling of the whole lower atmosphere. Unstable stratification of boundary layer suggests that aerosol-PBL interaction may not take much responsibility in haze formation during EP2. Notably, small warming in the surface layer of Figure 3b resulted possibly from anthropogenic heat flux as the BJ sounding station located at the downtown area of the city (Pascual et al., 2003).

3.3. Quantitative Understanding of Different Aerosol-PBL Interactions by Simulation

During COVID-19 lockdown period, anthropogenic emissions from all sources experienced drastic reduction (Figure S1). Numerical simulations which can well captured the variations of aerosols are incorporated to shed more light on the impact of emission reduction on aerosol-PBL interaction (Figures S6 and S7). The decreasing magnitude of column BC concentration reached 30%, almost the same as BC emission reduction (Figure S8). In contrast, the reductions in $PM_{2.5}$ precursors' emission were about 2 times of its reduction in concentrations over BTH, suggesting the nonlinear relationship of secondary pollution and its precursors. Accordingly, atmospheric AOD decreased by 0.2 and SSA increased by 0.02, indicative of a less absorbing atmosphere. The spatial variation of AOD resembles that of $PM_{2.5}$ column concentration quite well. It should be noted that the difference between two numerical experiments (CUT–noCUT) is only related to emission change under the same meteorological conditions after the lockdown implemented. But the comparison made using observations (Lock–Pre) are affected by both emission reduction and synoptic circulation, where AOD showed an increasing trend.

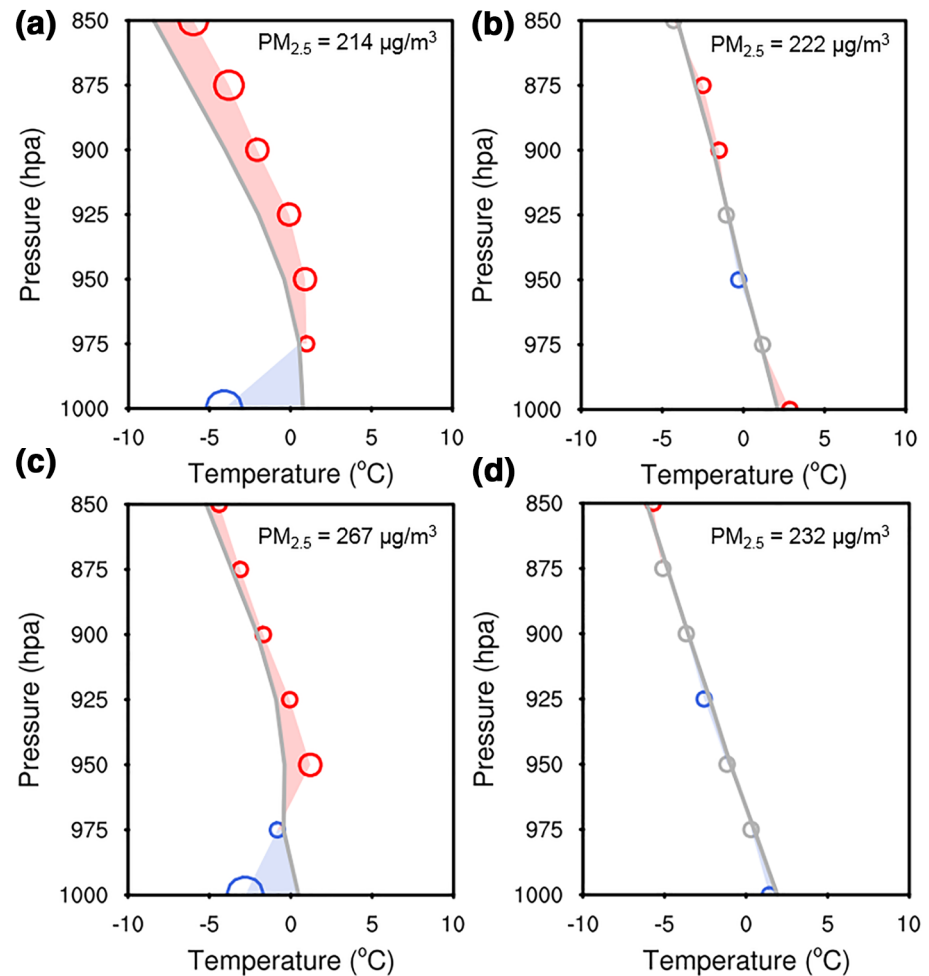


Figure 3. Comparison of temperature profile recorded by atmospheric sounding and GFS forecast at BJ ([a], [b]) and XT ([c], [d]) during prelockdown ([a], [c]) and lockdown period ([b], [d]). The gray lines represent the predicted stratification from GFS. The red, gray, and blue circles symbolize the observed values that are larger, approximate to, and smaller than predictions. The size of the circle denotes the relative magnitudes of the deviation. The geographic locations of BJ and XT are marked in Figure 1. The corresponding $PM_{2.5}$ concentration is marked at the top-right corner in each plot. GFS, Global Forecast System.

The effect of aerosol-PBL interaction on surface pollutants under the original emission scenario is quite apparent (Figure S9). As aforementioned, suspended aerosols would trap solar radiation within the atmosphere, resulting in a regional cooling at surface and a distinct heating at a higher altitude as large as $0.5^{\circ}C$. With more stabilized stratification, PBL was suppressed by about 200 m over northern and eastern China, which further increased near surface pollution by $40 \mu g/m^3$. On the other hand, due to reduction of primary aerosols after the lockdown, daytime atmospheric heating showed a $0.2^{\circ}C$ decreasing trend (Figure 4). Combined with more upward sensible heat flux, the development of PBL was enhanced by over 50 m. Ultimately, almost half of the pollution enhancement by aerosol-PBL interaction, approximate to $25 \mu g/m^3$, was alleviated under emission reduction scenario resulted from weakened feedback over polluted areas. A sensitivity experiment with all emission reduced except for BC indicates that BC dominates the atmospheric heating in the upper boundary layer and hence shallower PBL height due to increasing stability (Figure 4e). The reduction of BC only can lead to about $15 \mu g/m^3$ ($\sim 30\%$) decrease of $PM_{2.5}$ enhancement due to the weakened feedback, while other components can also make a difference. It is also worth noting that light-absorbing organic matter such as brown carbon (BrC) may contribute to the atmospheric heating and the feedback as well. However, due to limited absorption capacity of secondary organic aerosols (Z. Li et al., 2019; Saleh et al., 2013) and uncertainties in parameterizing optical properties of organic matter (Yao

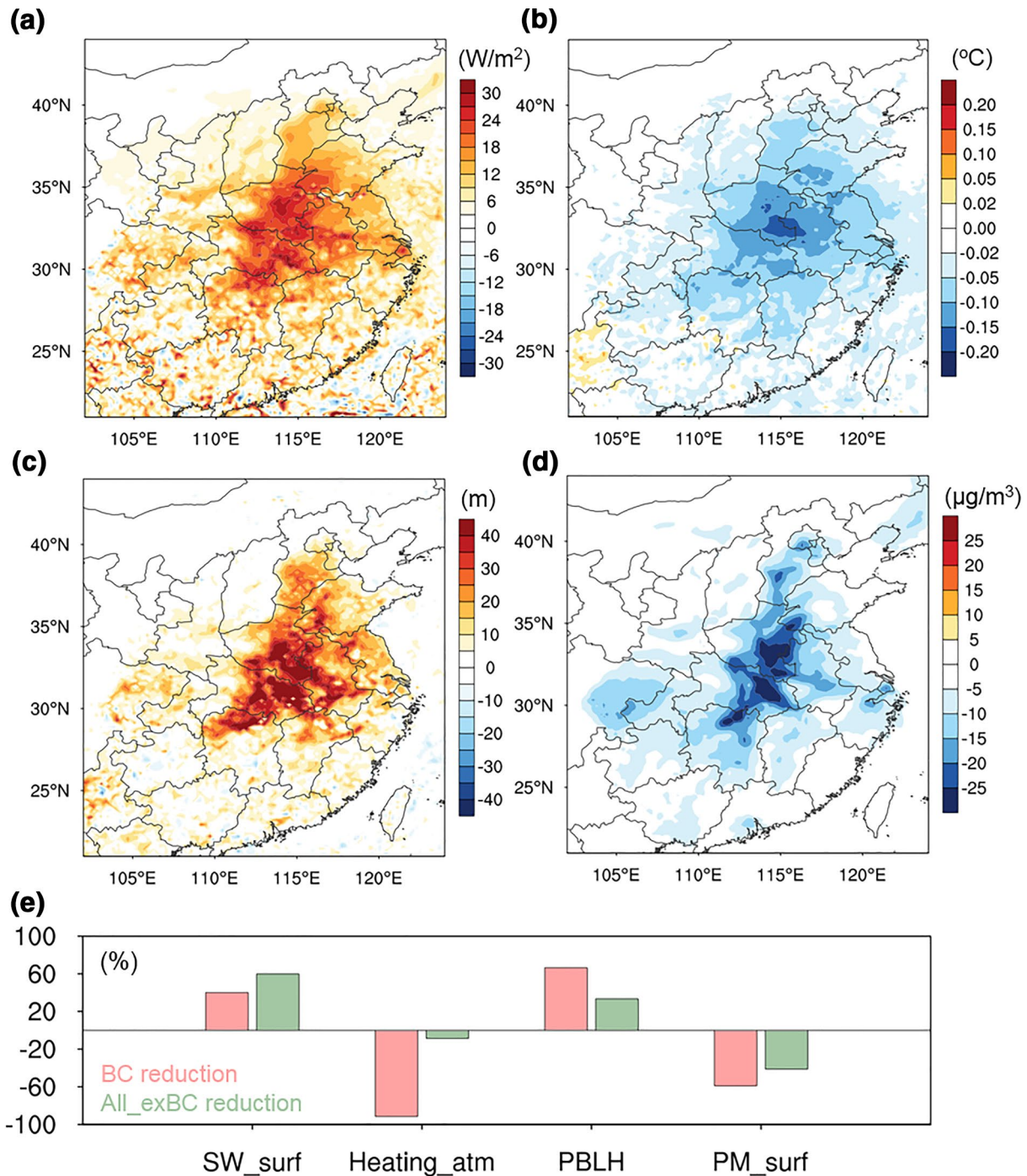


Figure 4. Alteration of atmospheric meteorological and chemical response to aerosol-PBL interaction caused by emission reduction during COVID-19 lockdown. (a) Incident shortwave radiation change at surface. (b) Atmospheric temperature change at 800 m. (c) Daytime PBL height change. (d) Surface PM_{2.5} concentration change. (e) The relative contributions from BC and other aerosol components to aerosol-PBL interaction in terms of changes in incoming shortwave radiation at surface (SW_surf), atmospheric heating (Heating_atm), PBL height, and surface PM_{2.5} concentration (PM_surf) over eastern China. BC, black carbon; PBL, planetary boundary layer.

et al., 2017), the role of BrC is not discussed in this study. In all, emission reduction during COVID-19 lockdown could mitigate the air pollution not only through direct source cut-down but also through weakened aerosol-PBL interaction effect, although the alleviation was partly offset by enhanced secondary pollution formation from meteorology and chemistry.

4. Conclusions

As COVID-19 pandemic spread globally, human activities and the associated anthropogenic emissions were greatly constrained. Strict restrictions on transportation and gathering were implemented in China since the outbreak of COVID-19 in the late January 2020. Nevertheless, high loadings of particles were still observed over BTH. Based on in situ measurements, we found that SNAO increased by 4, 2, 2, and 7 $\mu\text{g}/\text{m}^3$, respectively, on average, contributing greatly to the elevated $\text{PM}_{2.5}$. On the contrary, as the key factor of aerosol-PBL interaction, absorbing BC decreased by $\sim 10\%$ average over BTH. Overall, secondary aerosols with scattering effect (SNAO) took up an increasing percentage of $\text{PM}_{2.5}$, yet the fraction of primary absorbing BC exhibited a 50% reduction. In response to the changing aerosol composition, both atmospheric AOD and SSA increased, which resulted in AAOD falling by 60% from about 10×10^{-3} to 4×10^{-3} after the lockdown, indicative of a more scattering atmosphere. Comparison between weather forecast and radiosonde observations indicated that without upper-level heating induced by BC, lower surface cooling tended to diffuse and homogenize in the whole boundary layer. Stabilized stratification of aerosol-PBL interaction thus diminished, which is conducive for PBL mixing and hence near-surface pollution dispersion. Multiple parallel experiments conducted with WRF-Chem under different emission scenarios confirmed the dominant role of BC in atmospheric heating as well as suppressing PBL development. The enhancement of $\text{PM}_{2.5}$ resulted from aerosol-PBL interaction is alleviated by emission reduction with a magnitude of 25 $\mu\text{g}/\text{m}^3$ ($\sim 50\%$) through weakening the feedback, which would otherwise intensify the haze during the lockdown period. After observationally confirmed and numerically quantified the importance of BC-induced meteorological feedback, the work further highlights the priority of BC control as an efficient way to mitigate haze pollution in areas with intensive fossil fuel combustion like China. Also, the BC control policies may also benefit the environment for diminishing primary and secondary organic aerosols concurrently (Bergmann et al., 2009; Robinson et al., 2007).

Combining multiple observations and quantitative simulations, the study pictured the change of air pollutants especially aerosol components over BTH due to COVID-19 lockdown and analyzed its linkage to the variation of atmospheric optical properties. The quantitative role of BC and other components in the formation of stable stratification and haze aggravation had been further addressed by simulations with fixed and dynamic emission scenarios. Except for YSU, another two prevailing PBL schemes (MYJ and MYNN2.5) are also tested using single-column model and showed similar results with limited variations (Table S2). Nevertheless, there still remain some uncertainties in the simulation work. For example, internal mixing is assumed for all aerosols and throughout the entire simulation, yet how variations of aerosol composition can influence its mixing state is still unclear, which requires more observational and laboratory studies. Further, the optical properties of organic matter are poorly estimated in WRF-Chem model, calling for more detailed treatment of absorption caused by light-absorbing organic species such as BrC.

Data Availability Statement

Satellite-derived daily optical properties from MODIS can be ordered at http://dx.doi.org/10.5067/MODIS/MOD04_L2.006. Other data supporting the analysis and conclusions of this work are available at <https://doi.org/10.5281/zenodo.4001598>. No potential conflict of interest was reported by the authors.

Acknowledgments

This work was supported by the National Natural Science Foundation of China under grants 41922038 and 41725020.

References

- Barnard, J. C., Fast, J. D., Paredes-Miranda, G., Arnott, W. P., & Laskin, A. (2010). Technical note: Evaluation of the WRF-Chem "Aerosol chemical to aerosol optical properties" module using data from the MILAGRO campaign. *Atmospheric Chemistry and Physics*, 10(15), 7325–7340. <https://doi.org/10.5194/acp-10-7325-2010>
- Bauwens, M., Compornolle, S., Stavrakou, T., Müller, J.-F., Gent, J., Eskes, H., et al. (2020). Impact of Coronavirus outbreak on NO_2 pollution assessed using TROPOMI and OMI observations. *Geophysical Research Letters*, 47(11), e2020GL087978. <https://doi.org/10.1029/2020GL087978>
- Bergmann, M., Kirchner, U., Vogt, R., & Benter, T. (2009). On-road and laboratory investigation of low-level PM emissions of a modern diesel particulate filter equipped diesel passenger car. *Atmospheric Environment*, 43(11), 1908–1916. <https://doi.org/10.1016/j.atmosenv.2008.12.039>
- Bond, T. C., Doherty, S. J., Fahey, D. W., Forster, P. M., Berntsen, T., DeAngelo, B. J., et al. (2013). Bounding the role of black carbon in the climate system: A scientific assessment. *Journal of Geophysical Research: Atmospheres*, 118(11), 5380–5552. <https://doi.org/10.1002/jgrd.50171>
- Chang, Y., Huang, R.-J., Ge, X., Huang, X., Hu, J., Duan, Y., et al. (2020). Puzzling haze events in China during the coronavirus (COVID-19) shutdown. *Geophysical Research Letters*, 47(12), e2020GL088533. <https://doi.org/10.1029/2020GL088533>

- Chapman, E. G., Gustafson, W., Easter, R. C., Barnard, J. C., Ghan, S. J., Pekour, M. S., & Fast, J. D. (2009). Coupling aerosol–cloud–radiative processes in the WRF-Chem model: Investigating the radiative impact of elevated point sources. *Atmospheric Chemistry and Physics*, 9(3), 945–964. <https://doi.org/10.5194/acp-9-945-2009>
- Chen, H., Huo, J., Fu, Q., Duan, Y., Xiao, H., & Chen, J. (2020). Impact of quarantine measures on chemical compositions of PM_{2.5} during the COVID-19 epidemic in Shanghai, China. *Science of the Total Environment*, 743, 1–6. 140758. <https://doi.org/10.1016/j.scitotenv.2020.140758>
- Diamond, M. S., & Wood, R. (2020). Limited regional aerosol and cloud microphysical changes despite unprecedented decline in nitrogen oxide pollution during the February 2020 COVID-19 shutdown in China. *Geophysical Research Letters*, 47(17), e2020GL088913. <https://doi.org/10.1029/2020GL088913>
- Ding, A., Huang, X., Nie, W., Chi, X., Xu, Z., Zheng, L., et al. (2019). Significant reduction of PM_{2.5} in eastern China due to regional-scale emission control: Evidence from SORPES in 2011–2018. *Atmospheric Chemistry and Physics*, 19(18), 11791–11801. <https://doi.org/10.5194/acp-19-11791-2019>
- Ding, A. J., Huang, X., Nie, W., Sun, J. N., Kerminen, V.-M., Petäjä, T., et al. (2016). Enhanced haze pollution by black carbon in megacities in China. *Geophysical Research Letters*, 43(6), 2873–2879. <https://doi.org/10.1002/2016GL067745>
- Ek, M. B., Mitchell, K. E., Lin, Y., Rogers, E., Grunmann, P., Koren, V., et al. (2003). Implementation of Noah land surface model advances in the National Centers for Environmental Prediction operational mesoscale Eta model. *Journal of Geophysical Research*, 108(D22), 8851–8866. <https://doi.org/10.1029/2002JD003296>
- Fast, J. D., Gustafson, W. I., Easter, R. C., Zaveri, R. A., Barnard, J. C., Chapman, E. G., et al. (2006). Evolution of ozone, particulates, and aerosol direct radiative forcing in the vicinity of Houston using a fully coupled meteorology–chemistry–aerosol model. *Journal of Geophysical Research*, 111(D21), 305–333. <https://doi.org/10.1029/2005JD006721>
- Filonchyk, M., Hurynovich, V., Yan, H., Gusev, A., & Shpilevskaya, N. (2020). Impact assessment of COVID-19 on variations of SO₂, NO₂, CO and AOD over East China. *Aerosol and Air Quality Research*, 20(7), 1530–1540. <https://doi.org/10.4209/aaqr.2020.05.0226>
- Forkel, R., Werhahn, J., Hansen, A., McKeen, S., Peckham, S., Grell, G., & Suppan, P. (2012). Effect of aerosol–radiation feedback on regional air quality—A case study with WRF/Chem. *Atmospheric Environment*, 53, 202–211. <https://doi.org/10.1016/j.atmosenv.2011.10.009>
- Fu, X., Wang, T., Gao, J., Wang, P., Liu, Y., Wang, S., et al. (2020). Persistent heavy winter nitrate pollution driven by increased photochemical oxidants in Northern China. *Environmental Science & Technology*, 54(7), 3881–3889. <https://doi.org/10.1021/acs.est.9b07248>
- Grell, G. A., Freitas, S. R., Stuefer, M., & Fast, J. (2011). Inclusion of biomass burning in WRF-Chem: Impact of wildfires on weather forecasts. *Atmospheric Chemistry and Physics*, 11(11), 5289–5303. <https://doi.org/10.5194/acp-11-5289-2011>
- Grell, G. A., & Dévényi, D. (2002). A generalized approach to parameterizing convection combining ensemble and data assimilation techniques. *Geophysical Research Letters*, 29(14), 1693–1696. <https://doi.org/10.1029/2002GL015311>
- Hong, S. Y., Noh, Y., & Dudhia, J. (2006). A new vertical diffusion package with an explicit treatment of entrainment processes. *Monthly Weather Review*, 134(9), 2318–2341. <https://doi.org/10.1175/mwr3199.1>
- Huang, X., Ding, A., Gao, J., Zheng, B., Zhou, D., Qi, X., et al. (2020a). Enhanced secondary pollution offset reduction of primary emissions during COVID-19 lockdown in China. *National Science Review*, 0, 1–9. <https://doi.org/10.1093/nsr/nwaa137>
- Huang, X., Ding, A., Wang, Z., Ding, K., Gao, J., Chai, F., & Fu, C. (2020b). Amplified transboundary transport of haze by aerosol–boundary layer interaction in China. *Nature Geoscience*, 13, 428–434. <https://doi.org/10.1038/s41561-020-0583-4>
- Huang, X., Song, Y., Zhao, C., Cai, X., Zhang, H., & Zhu, T. (2015). Direct radiative effect by multicomponent aerosol over China. *Journal of Climate*, 28(9), 3472–3495. <https://doi.org/10.1175/JCLI-D-14-00365.1>
- Huang, X., Wang, Z., & Ding, A. (2018). Impact of aerosol–PBL interaction on haze pollution: Multiyear observational evidences in North China. *Geophysical Research Letters*, 45(7020), 8596–8603. <https://doi.org/10.1029/2018GL079239>
- Iacono, M. J., Delamere, J. S., Mlawer, E. J., Shephard, M. W., Clough, S. A., & Collins, W. D. (2008). Radiative forcing by long-lived greenhouse gases: Calculations with the AER radiative transfer models. *Journal of Geophysical Research*, 113(D13), 103–110. <https://doi.org/10.1029/2008JD009944>
- Jia, M., Zhao, T., Cheng, X., Gong, S., Zhang, X., Tang, L., et al. (2017). Inverse relations of PM_{2.5} and O₃ in air compound pollution between cold and hot seasons over an urban area of East China. *Atmosphere*, 8(3), 59. <https://doi.org/10.3390/atmos8030059>
- Li, K., Jacob, D. J., Liao, H., Shen, L., Zhang, Q., & Bates, K. H. (2019a). Anthropogenic drivers of 2013–2017 trends in summer surface ozone in China. *Proceedings of the National Academy of Sciences*, 116(2), 422–427. <https://doi.org/10.1073/pnas.1812168116>
- Li, M., Zhang, Q., Streets, D. G., He, K. B., Cheng, Y., Emmons, L. K., et al. (2014). Mapping Asian anthropogenic emissions of non-methane volatile organic compounds to multiple chemical mechanisms. *Atmospheric Chemistry and Physics*, 14(11), 5617–5638. <https://doi.org/10.5194/acp-14-5617-2014>
- Li, Z., Guo, J., Ding, A., Liao, H., Liu, J., Sun, Y., et al. (2017). Aerosol and boundary-layer interactions and impact on air quality. *National Science Review*, 4(6), 810–833. <https://doi.org/10.1093/nsr/nwx117>
- Li, Z., Tan, H., Zheng, J., Liu, L., Qin, Y., Wang, N., et al. (2019b). Light absorption properties and potential sources of particulate brown carbon in the Pearl River Delta region of China. *Atmospheric Chemistry and Physics*, 19(18), 11669–11685. <https://doi.org/10.5194/acp-19-11669-2019>
- Lin, Y.-L., Farley, R. D., & Orville, H. D. (1983). Bulk parameterization of the snow field in a cloud model. *Journal of Climate and Applied Meteorology*, 22(6), 1065–1092. <https://doi.org/10.1175/1520-0450%281983%29022%2C1065:BPOTSF%2E0.CO;2>
- Miao, Y., Guo, J., Liu, S., Liu, H., Li, Z., Zhang, W., & Zhai, P. (2017). Classification of summertime synoptic patterns in Beijing and their associations with boundary layer structure affecting aerosol pollution. *Atmospheric Chemistry and Physics*, 17(4), 3097–3110. <https://doi.org/10.5194/acp-17-3097-2017>
- Moise, T., Flores, M., & Rudich, Y. (2015). Optical properties of secondary organic aerosols and their changes by chemical processes. *Chemical Reviews*, 115(10), 4400–4439. <https://doi.org/10.1021/cr5005259>
- Nichol, J. E., Bilal, M., Ali, M. A., & Qiu, Z. (2020). Air pollution scenario over China during COVID-19. *Remote Sensing*, 12(13), 2100–2111. <https://doi.org/10.3390/rs12132100>
- Pascual, J. I., Lorente, N., Song, Z., Conrad, H., & Rust, H.-P. (2003). Selectivity in vibrationally mediated single-molecule chemistry. *Nature*, 423(6939), 525–528. <https://doi.org/10.1038/nature01649>
- Pei, Z., Han, G., Ma, X., Su, H., & Gong, W. (2020). Response of major air pollutants to COVID-19 lockdowns in China. *Science of the Total Environment*, 743, 140879. <https://doi.org/10.1016/j.scitotenv.2020.140879>
- Ramanathan, V., & Carmichael, G. (2008). Global and regional climate changes due to black carbon. *Nature Geoscience*, 1(4), 221–227. <https://doi.org/10.1038/ngeo156>
- Robinson, A. L., Donahue, N. M., Shrivastava, M. K., Weitkamp, E. A., Sage, A. M., Grieshop, A. P., et al. (2007). Rethinking organic aerosols: Semivolatile emissions and photochemical aging. *Science*, 315(5816), 1259–1262. <https://doi.org/10.1126/science.1133061>

- Saleh, R., Hennigan, C. J., McMeeking, G. R., Chuang, W. K., Robinson, E. S., Coe, H., et al. (2013). Absorptivity of brown carbon in fresh and photo-chemically aged biomass-burning emissions. *Atmospheric Chemistry and Physics*, *13*(15), 7683–7693. <https://doi.org/10.5194/acp-13-7683-2013>
- Sun, Y., Lei, L., Zhou, W., Chen, C., He, Y., Sun, J., et al. (2020). A chemical cocktail during the COVID-19 outbreak in Beijing, China: Insights from six-year aerosol particle composition measurements during the Chinese New Year holiday. *Science of the Total Environment*, *742*, 140739. <https://doi.org/10.1016/j.scitotenv.2020.140739>
- Wang, N., Lyu, X., Deng, X., Huang, X., Jiang, F., & Ding, A. (2019a). Aggravating O₃ pollution due to NO_x emission control in eastern China. *The Science of the Total Environment*, *677*, 732–744. <https://doi.org/10.1016/j.scitotenv.2019.04.388>
- Wang, P., Chen, K., Zhu, S., Wang, P., & Zhang, H. (2020). Severe air pollution events not avoided by reduced anthropogenic activities during COVID-19 outbreak. *Resources, Conservation and Recycling*, *158*, 104814. <https://doi.org/10.1016/j.resconrec.2020.104814>
- Wang, Z., Huang, X., & Ding, A. (2018). Dome effect of black carbon and its key influencing factors: A one-dimensional modeling study. *Atmospheric Chemistry and Physics*, *18*(4), 2821–2834. <https://doi.org/10.5194/acp-18-2821-2018>
- Wang, Z., Huang, X., & Ding, A. (2019b). Optimization of vertical grid setting for air quality modeling in China considering the effect of aerosol–boundary layer interaction. *Atmospheric Environment*, *210*, 1–13. <https://doi.org/10.1016/j.atmosenv.2019.04.042>
- Yao, H., Song, Y., Liu, M., Archer-Nicholls, S., Lowe, D., McFiggans, G., et al. (2017). Direct radiative effect of carbonaceous aerosols from crop residue burning during the summer harvest season in East China. *Atmospheric Chemistry and Physics*, *17*(8), 5205–5219. <https://doi.org/10.5194/acp-17-5205-2017>
- Zaveri, R. A., Easter, R. C., Fast, J. D., & Peters, L. K. (2008). Model for Simulating Aerosol Interactions and Chemistry (MOSAIC). *Journal of Geophysical Research*, *113*(D13), 204–232. <https://doi.org/10.1029/2007JD008782>
- Zaveri, R. A., & Peters, L. K. (1999). A new lumped structure photochemical mechanism for large-scale applications. *Journal of Geophysical Research*, *104*(D23), 30387–30415. <https://doi.org/10.1029/1999JD900876>
- Zhang, R., Zhang, Y., Lin, H., Feng, X., Fu, T.-M., & Wang, Y. (2020). NO_x emission reduction and recovery during COVID-19 in East China. *Atmosphere*, *11*(4), 433–447. <https://doi.org/10.3390/atmos11040433>
- Zheng, B., Geng, G., Ciais, P., Davis, S. J., Martin, R., Meng, J., et al. (2020). Satellite-based estimates of decline and rebound in China's CO₂ emissions during COVID-19 pandemic. *New England Journal of Medicine*, *382*(8), 727–733. <https://doi.org/10.1056/NEJMoa2001017>
- Zhu, N., Zhang, D., Wang, W., Li, X., Yang, B., Song, J., et al. (2020). A novel Coronavirus from patients with pneumonia in China, 2019. *New England Journal of Medicine*, *382*(8), 727–733. <https://doi.org/10.1056/NEJMoa2001017>